

An Attention-Assisted AI Model for Real-Time Underwater Sound Speed Estimation Leveraging Remote Sensing Sea Surface Temperature Data

Pengfei Wu, Wei Huang*, *Member, IEEE*, Yujie Shi, Hao Zhang, *Senior Member, IEEE*

Abstract—The estimation of underwater sound velocity distribution serves as a critical basis for facilitating effective underwater communication and precise positioning, given that variations in sound velocity influence the path of signal transmission. Conventional techniques for the direct measurement of sound velocity, as well as methods that involve the inversion of sound velocity utilizing acoustic field data, necessitate on-site data collection. This requirement not only places high demands on device deployment, but also presents challenges in achieving real-time estimation of sound velocity distribution. In order to construct a real-time sound velocity field and eliminate the need for underwater onsite data measurement operations, we propose a self-attention embedded multimodal data fusion convolutional neural network (SA-MDF-CNN) for real-time underwater sound speed profile (SSP) estimation. The proposed model seeks to elucidate the inherent relationship between remote sensing sea surface temperature (SST) data, the primary component characteristics of historical SSPs, and their spatial coordinates. This is achieved by employing CNNs and attention mechanisms to extract local and global correlations from the input data, respectively. The ultimate objective is to facilitate a rapid and precise estimation of sound velocity distribution within a specified task area. The comparative analysis demonstrates that the proposed approach achieves superior performance in terms of both accuracy and stability, exhibiting reduced error rates and enhanced resistance to disturbances when benchmarked against existing advanced techniques.

Index Terms—self-attention, multimodal data fusion, convolutional neural network (CNN), real-time underwater sound speed profile (SSP) estimation, remote sensing sea surface temperature (SST) data.

I. INTRODUCTION

UNDERWATER sound velocity construction plays an indispensable role in many applications such as underwater positioning, navigation, timing, communication (PNTC) and target recognition due to its decisive factor in the signal propagation mode [1]–[3]. Acoustic propagation speed in marine settings exhibits spatial variability due to the combined effects of temperature, salinity, and pressure [4]–[7]. Generally, the

sound velocity exhibits a stratified variation with depth, so that sound speed profiles (SSPs) are commonly employed to describe the distribution of sound velocity.

The methodology for acquiring SSPs has been a popular research topic for a long period. In traditional ways, SSPs can be directly measured using various instruments, including the conductivity–temperature–depth profiler (CTD), the expendable CTD (XCTD), and the sound velocity profiler (SVP). Alternatively, SSPs can be derived by inversion based on acoustic field data, which encompasses parameters such as signal transmission time or received signal strength [8]–[12]. In general, instrument-based measurements can provide precise SSPs with high–depth resolution, but the measurement process is notably time-intensive. For instance, when the instrument is deployed at a regular speed of 50 meters per minute, it takes at least 80 minutes to measure the sound velocity value within a depth range of 2000 meters to complete the deployment and retrieval of the equipment [11]. As a result, it is difficult to provide real-time sound velocity distributions for underwater communication and positioning through instrument-based measurement. Considering that the distribution of sound velocity can affect the distribution of sound field, researchers have proposed a series of methods to invert the sound velocity distribution by using on-site measured sound field data such as signal propagation time in order to accelerate the process of obtaining sound velocity. There are three main frameworks for inversion methods, including matching field processing (MFP) [13], compressive sensing (CS) [14], [15], and deep learning (DL) [4], [16]. The proposed inversion technique enables fast acquisition of sound speed profiles, offering substantial temporal advantages over conventional conductivity–temperature–depth (CTD) sensors and sound velocity profilers (SVPs) in marine data collection. However, because of the interference of noise in sound field measurement, there is a loss in the accuracy of these sound velocity inversion methods. More importantly, it still takes a certain amount of time to measure the sound field data, and new requirements have been put forward for the deployment of expensive sound field measurement equipment. The implementation of SSP inversion techniques is inherently constrained by their dependence on active sonar measurements, thereby limiting their applicability in regions beyond the operational range of underwater acoustic monitoring networks.

Over the past few years, the fast development of underwater automated sensing equipment has provided increasingly rich vertical observation reference data for exploring the

Manuscript received XX XX, 2025; revised XX XX, XXXX.

This work was supported in part by the National Natural Science Foundation of China under Grant 42404001 and 62271459, in part by Natural Science Foundation of Shandong Province under Grant ZR2023QF128, and in part by the Fundamental Research Funds for the Central Universities, Ocean University of China under Grant 202313036.

Pengfei Wu, Hao Zhang, and Wei Huang are with the College of Electronic Engineering, Yujie Shi is from the School of Environmental Science and Engineering, Ocean University of China, Qingdao, Shandong 266404, China (email: wupengfei@stu.ouc.edu.cn; zhanghao@ouc.edu.cn).

Corresponding author: Wei Huang (email:hw@ouc.edu.cn). Pengfei Wu, Wei Huang and Yujie Shi contributed equally to this work.

distribution of underwater sound velocity. To achieve fast estimation of SSPs and eliminate the need for underwater on-site operations, various methods have emerged that use empirical sound velocity distribution data or remote sensing data. [17]–[19] utilize empirical SSPs data to capture the changes in sound velocity from a time series perspective, enabling real-time estimation and prediction of sound velocity distribution in designated ocean areas. These SSP prediction methods have a single type of input data and low complexity of model construction. However, because of the low time resolution of historical samples, its accuracy performance is not good enough in estimating the sound velocity within a small-scale time range. In fact, the variation of sound velocity distribution in a small-scale spatial area is mainly reflected in the shallow water part, as it is more significantly affected by temperature changes. Marine remote sensing technology provides real-time and reliable high spatiotemporal resolution sea surface temperature (SST) data [20], which can offer initial sea surface condition constraints for estimating underwater sound velocity distribution. [21] proposed a self-organizing map (SOM) neural network model that combines empirical sound velocity data and remote sensing SST data, but the model mainly focuses on the local characteristics of sound velocity distribution, which not only fails to capture the influence of SST data on deep ocean sound velocity, but also fails to capture the spatial correlation of sound velocity distribution. As a result, the accuracy performance has not been significantly improved compared to prediction methods.

In order to fast and accurately estimate the SSP of a given task area without on-site underwater data measurement, we propose an interpretable self-attention-assisted multimodal data fusion convolutional neural network (SA-MDF-CNN) model in this paper to deeply capture the intrinsic relationships among empirical SSP data, remote sensing SST data, and spatial coordinates. The core idea is to capture the local feature correlation of regional sound velocity distribution through CNN, and enhance the learning ability of global feature correlation of multimodal data through attention mechanism. To evaluate the effectiveness of the proposed SA-MDF-CNN model, we conducted experiments using Argo data from the Pacific Ocean and measured data from the South China Sea in 2023. Results show that SA-MDF-CNN can achieve lower root mean square error (RMSE) than other spatial SSP construction methods. The contribution of this paper can be summarized as follows:

- To achieve real-time estimation of SSP without on-site underwater data measurement, we propose an attention-assisted multimodal data fusion convolutional neural network (SA-MDF-CNN) model. We take into account the mutual influence among empirical sound velocity distribution, SST, and spatial position, and the attention module is designed to enhance the global feature learning ability of the model.
- To evaluate the accuracy performance of the model, we conducted experiments using Argo data from the Pacific region and further validated it through sea trials in the South China Sea in 2023. The RMSE of both experimen-

tal results is superior to other spatial SSP constructing methods.

- To enhance the interpretability of the model, the weights of the model parameters are visualized. As the number of training iterations increases, the model parameter weights gradually focus on the shallow water part. This is reasonable because through the empirical orthogonal function (EOF) decomposition of historical SSPs, it can be seen that the differences in sound velocity distribution are more prominent in shallow water. Therefore, the weight visualization results indicate that the model can effectively capture the characteristics of sound velocity distribution.

The structure of this article is arranged as follows. Section 2 provides a detailed introduction to relevant works. The overall architecture and functional module description of the SA-MDF-CNN model are provided in Section 3. Section 4 gives the experimental findings, and the final section, Section 5, presents the concluding remarks.

II. RELATED WORKS

The distribution of underwater sound velocity plays an essential role in the energy distribution and propagation trajectory of acoustic signals. Therefore, real-time and accurate estimation of sound velocity distribution has significant value for applications based on communication and positioning technologies such as underwater PNTC systems, and target recognition systems.

The traditional way of obtaining sound velocity distribution is usually through direct measurement using shipborne CTD or SVP equipment, which has the advantage of high accuracy [22], [23]. However, it comes with high economic costs and measurement time expenses. With the development of sensing and network technology, many kinds of underwater environmental observation systems have been established to enhance human understanding of the ocean. In 1979, MUNK and Wunsch first put forward the concept of ocean acoustic tomography that using acoustic field observation information to invert the sound velocity distribution [24], [25]. Since then, there have been three mainstream frameworks for sound velocity inversion, namely MFP [13], CS [14], [15], and DL [4], [16]. The MFP framework mainly consists of four steps. Firstly, EOF decomposition is adopted to extract the principal component features of the regional sound velocity distribution. Then, different feature combinations are generated to form candidate SSPs. Next, the sound field distribution is simulated based on ray theory. Finally, the simulated sound field is matched with the measured sound field to determine the optimal estimation of SSP. To accelerate the search speed of the optimal candidate SSP, Tolstoy introduced simulated annealing algorithm in the MFP, which improved the algorithm execution efficiency but resulted in suboptimal solutions [13]. Afterwards, other heuristic algorithms were combined with MFP frameworks for SSP inversion, but they also obtained suboptimal solutions [26], [27]. To further improve the efficiency of inversion algorithm execution, Bianco [15] and Choo [14] proposed SSP inversion framework based on CS,

respectively. In the CS framework, the mapping relationship from the sound field distribution to the sound velocity distribution is established through a matrix, which eliminates the search process for matching terms. However, the matrix relationship introduces linear approximation, thus sacrificing inversion accuracy.

In recent years, deep learning theory has developed rapidly and achieved significant results in constructing unknown non-linear relationships between different data [28], [29]. In addition, long-term underwater environmental observations have accumulated a large amount of data for marine hydrological research, laying a data foundation for the application of deep learning underwater. To address the drawbacks of computational efficiency and accuracy loss in MFP and CS frameworks, we proposed a auto-encoding feature mapping neural network model for SSP inversion in our early work [4], in which the auto-encoder was created to extract deep robust features so as to reduce the impact of acoustic field measurement errors on the accuracy of sound velocity inversion. Considering the insufficient accumulation of historical sound velocity data in some ocean areas, the DL model is prone to over-fitting and reduces accuracy performance. Therefore, we further propose a few-shot meta learning framework to accelerate the convergence speed of the model [16]. However, the above-mentioned methods based on MFP, CS, and DL all rely on real-time measured acoustic field data, which puts high demands on the deployment of underwater observation equipment. Therefore, these methods not only face high equipment economic costs, but also have limited application scope for areas without sonar measurement systems.

Nowadays, how to eliminate the need for underwater on-site data measurement has become a research hotspot in the field of SSP inversion. Based on this requirement, Liu et al. and Lu et al. both proposed a long-short term memory (LSTM) neural network model for SSP prediction [17], [18], which only requires empirical SSP data. However, due to the low temporal resolution of prior data in most marine areas, this prediction method can only describe the overall trend of sound velocity changes and is difficult to obtain high-precision SSP prediction results. In fact, the SSP estimation methods, that rely on a single data modality (sound field data or historical SSP data), are susceptible to data quality issues, such as high sound field measurement noise or low sound velocity sampling time resolution. To improve the robustness of the sound velocity estimation model, researchers have proposed some multimodal data fusion methods for estimating sound velocity that combining data from different sensors and sources to obtain more comprehensive features than a single data source [21], [30]. Yu et al. proposed a radial basis function (RBF) neural network for SSP estimation that mainly using historical temperature, salinity profile data and average SSP data. Nevertheless, the model is not sensitive to varieties of sound velocity, and the estimation results often approach the average SSP profile, making it difficult to accurately describe the spatiotemporal distribution changes of sound velocity. Xu et al. proposed a physics-inspired SOM model for SSP estimation, which introduced remote sensing SST data. However, SOM can only capture the influence of

sea surface temperature on surface sound velocity distribution, and lacks the ability to capture large-scale feature correlations. Therefore, the accuracy of sound velocity estimation is difficult to meet practical application requirements.

To obtain real-time and accurate estimation of sound velocity distribution without underwater on-site data measurement, we fully consider the historical sound velocity distribution patterns of different spatial coordinates, as well as the impact of real-time SST changes on the dynamic characteristics of sound velocity distribution, and propose an interpretable SA-MDF-CNN model. In this model, the local correlation of features will be captured through CNN and global correlation of features will be captured through attention mechanism.

III. SA-MDF-CNN STRUCTURE FOR SSP ESTIMATION

To realize real-time and accurate estimation of sound velocity distribution, we propose an SSP estimation structure based on SA-MDF-CNN, which is shown in figure 1. In this paper, the ocean area of 5.5°N-45.5°N and 150.5°E-170.5°E are selected as the research scope. The remote sensing SST data, latitude and longitude coordinates, and the first three order feature vectors of historical SSPs decomposed by EOFs are first fused to construct the fusion data as the SA-MDF-CNN training data. Then, the multimodal fusion data of 8 grids around the task region is combined to construct the target SSP through the proposed SA-MDF-CNN model. In the following part, we will provide detailed introductions to data sources, data fusion structures, and the composition of neural network model, separately.

A. Data sources

Remote sensing SST data are provided by the National Oceanic and Atmospheric Administration (NOAA) [31] with a spatial grid resolution of 0.25° and a temporal resolution of 1 day. The SSP data are obtained from the Chinese Observation and Research Station for Global Ocean Argo System (Hangzhou) [32] with a spatial grid resolution of 1° and a temporal resolution of 1 month. Based on the objective analysis method of gradient-dependent correlation scale optimal interpolation, the 3D grid data of the subsurface layer (5-2000 meters) that covering 179.5°W to 179.5°E and 89.5°S to 89.5°N was constructed, and the observation profile was vertically interpolated to 57 standard layers with unequal intervals.

B. Fusion data construction

In the selected ocean region, we grid the entire area into N longitude-scales of 1°, M latitude-scales of 1°, and vertical depth of H layers. For any coordinate in the grid, the grid remote sensing SST data are expressed as $T_{n,m}^s$, and the monthly average SSP data of the historical period are chosen for data fusion, with the depth of the h th layer expressed as $D_{n,m}^h, n \in N, m \in M$.

Within the divided $N * M$ grid ocean area, each sub-grid ψ with a size of $3 * 3$ forms a set of training data, and each set of training data will be further divided into input data X

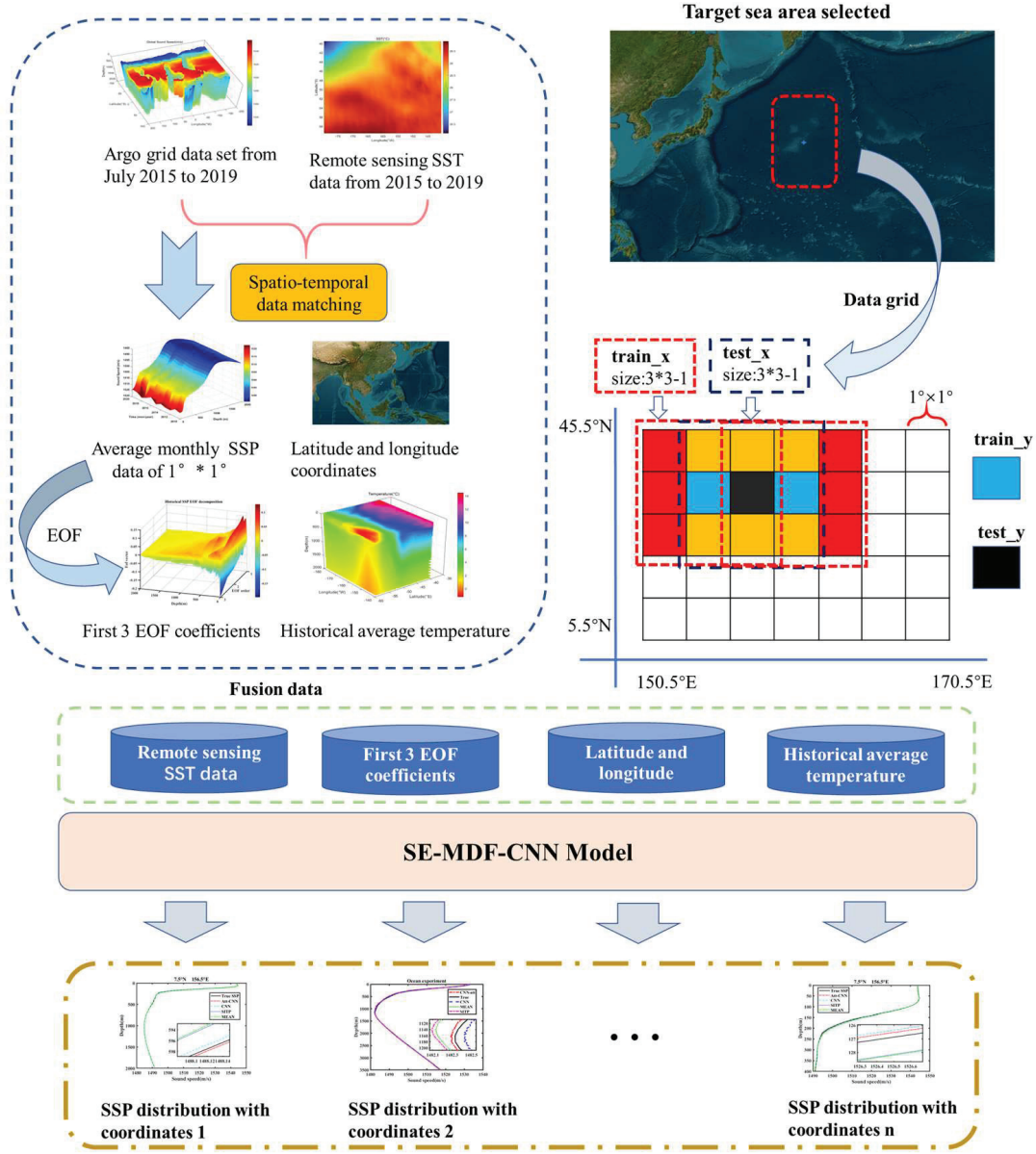


Fig. 1. SSP Estimation Structure based on SA-MDF-CNN.

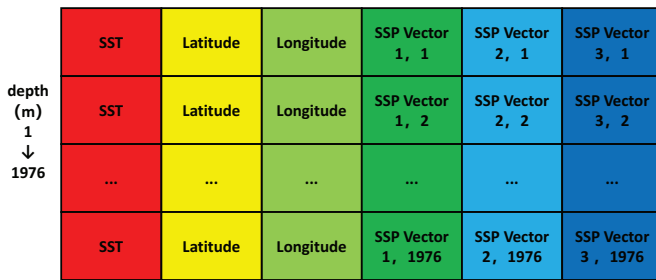


Fig. 2. The data fusion structure for a single coordinate.

and output label data Y , with a sliding step of 1 for each sub grid, as shown in Figure 1. Specifically, for a sub-grid ψ , the fusion data formed by 8 surrounding coordinates will be

the input data X , and the center SSP of each sub-grid ψ will be taken as the output label Y . If the coordinate of the grid center is $L_Y = L_{n,m}$, then the coordinates of the input data are represented as:

$$\mathcal{L}_X = [L_{n-1,m-1}, L_{n-1,m}, L_{n-1,m+1}, L_{n,m-1}, L_{n,m+1}, L_{n+1,m-1}, L_{n+1,m}, L_{n+1,m+1}], \quad n \in N, \quad m \in M. \quad (1)$$

For a single coordinate, the data fusion structure is shown in figure 2, which includes the real-time SST data, latitude and longitude coordinates, and the first three EOF feature vectors of the historical SSPs. EOF decomposition, also known as principal component analysis, is a statistical method used to analyze structural features in matrix data and extract major data feature quantities. Through EOF decomposition, the change information of the original sound velocity field can be

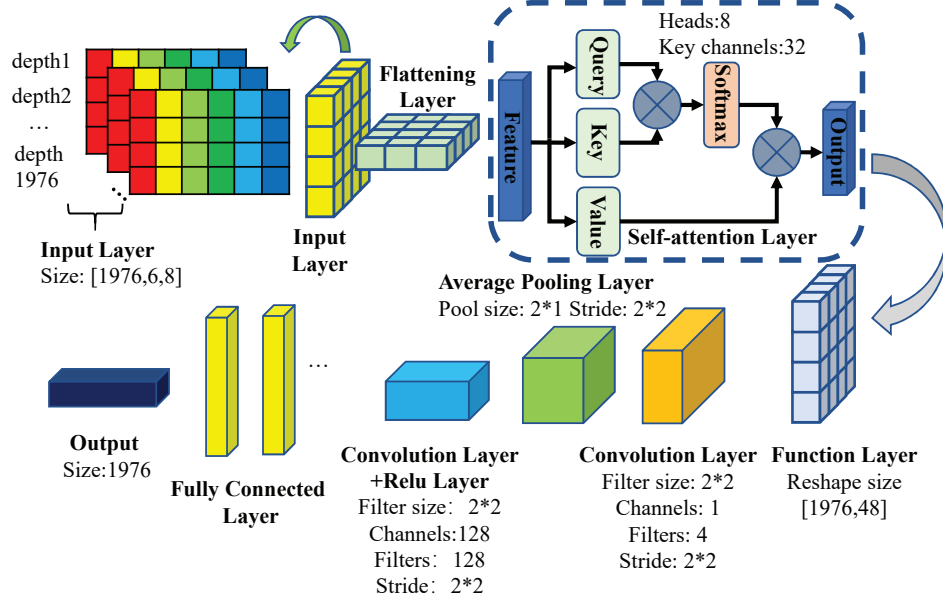


Fig. 3. SA-MDF-CNN model.

easily condensed into the first few principal components and their corresponding spatial functions, so the main information of the sound velocity field can be expressed only by the first few eigenvectors.

To obtain the EOF feature vectors, corresponding 5-year (2015 to 2019) historical SSPs from the target ocean area are first selected and then linearly interpolated with a step size of 1 m. This standardized interpolation is used to more clearly describe the differences in sound velocity values at different depths. Suppose there are J SSPs, and the j th SSP is expressed as a vector $\mathbf{S}_j = [s_{j,1}, s_{j,2}, \dots, s_{j,h}]^T$, $h = 1, 2, \dots, H$, $H = 1976$, where $s_{j,h}$ means the sound velocity value at the h th depth layer of the j th SSP. Since the SSP has been linearly interpolated, the depth of the h th depth layer is h m. Then, the matrix formed by all empirical SSPs will be:

$$\mathbf{S}_{\mathcal{H},\mathcal{J}} = \begin{bmatrix} s_{1,1} & s_{2,1} & \cdots & s_{J,1} \\ s_{1,2} & s_{2,2} & \cdots & s_{J,2} \\ \vdots & \vdots & \ddots & \vdots \\ s_{1,h} & s_{2,h} & \cdots & s_{J,h} \end{bmatrix}. \quad (2)$$

Based on equation (2), the average SSP $\mathbf{S}_0 = [s_{0,1}, s_{0,2}, \dots, s_{0,h}]^T$ can be calculated by averaging each row of equation (2). Next, a residual matrix can be constructed by subtracting \mathbf{S}_0 from each column of equation (2):

$$\mathbf{S}_{\mathcal{H},\mathcal{J}}^{\mathcal{R}} = [\mathbf{S}_1 - \mathbf{S}_0, \mathbf{S}_2 - \mathbf{S}_0, \dots, \mathbf{S}_J - \mathbf{S}_0]. \quad (3)$$

According to equation $\mathbf{S}_{\mathcal{H},\mathcal{J}}^{\mathcal{R}}$, the covariance matrix $\mathcal{C}_{\mathcal{H},\mathcal{H}}$ of sound velocity can be constructed as:

$$\mathcal{C}_{\mathcal{H},\mathcal{H}} = \frac{1}{J} \mathbf{S}_{\mathcal{J},\mathcal{H}}^{\mathcal{R}} * \mathbf{S}_{\mathcal{J},\mathcal{H}}^{\mathcal{R}T}, \quad (4)$$

where $\mathcal{C}_{\mathcal{H},\mathcal{H}}$ is a matrix with orders of $H \times H$. Performing EOF decomposition on $\mathcal{C}_{\mathcal{H},\mathcal{H}}$ yields eigenvectors and eigenvector coefficients:

$$\mathcal{C}_{\mathcal{H},\mathcal{H}} \times \mathcal{E}_{\mathcal{H},\mathcal{H}} = \lambda_{\mathcal{H}*\mathcal{H}} \times \mathcal{E}_{\mathcal{H},\mathcal{H}}, \quad (5)$$

where $\mathcal{E}_{\mathcal{H},\mathcal{H}}$ is the matrix composed by eigenvectors, and $\lambda_{\mathcal{H}*\mathcal{H}}$ is the matrix composed by eigenvalues. When sorting the eigenvector coefficients from large to small, the corresponding eigenvectors form the first few order eigenvectors.

For the j th SSP in $\mathcal{S}_{\mathcal{H},\mathcal{J}}$, it can be recovered by:

$$\mathbf{S}_j = \mathbf{S}_0 + \sum_{k=1}^K \alpha_k \mathbf{e}_k, \quad (6)$$

where \mathbf{e}_k means the k th eigenvector, and α_k is the corresponding coefficient that determines the proportion of the eigenvector. When an SSP is given as $\mathbf{S}_{tar} = [s_{tar,1}, s_{tar,2}, \dots, s_{tar,h}]^T$, $h = 1, 2, \dots, H$, the residual vector will be $\mathbf{S}_{\mathcal{H},\mathcal{TAR}}^{\mathcal{R}} = [\mathbf{S}_{tar} - \mathbf{S}_0]$. The vector of coefficients $\alpha = [\alpha_1, \alpha_2, \dots, \alpha_K]^T$ can be obtained by projecting the target SSP onto the first k eigenvectors of $\mathcal{E}_{\mathcal{H},\mathcal{H}}$:

$$\alpha = \mathcal{E}_{\mathcal{H},\mathcal{K}}^T \times \mathbf{S}_{\mathcal{H},\mathcal{TAR}}^{\mathcal{R}}. \quad (7)$$

Finally, by fusing data from 8 coordinate points, input training data can be obtained. For location $L_{n-1,m-1}$, the fused data input $\mathcal{F}_{n-1,m-1}^X$ can be expressed as:

$$\mathcal{F}_{n-1,m-1}^X = [\mathbf{T}_{n-1,m-1}^S, \mathbf{L}_{n-1,m-1}, \mathcal{E}_{\mathcal{H},\mathcal{K}}], \quad (8)$$

where $\mathbf{T}_{n-1,m-1}^S = [T_{n-1,m-1,1}^s, T_{n-1,m-1,2}^s, \dots, T_{n-1,m-1,H}^s]^T$ is actually a vector composed of H copies of $T_{n-1,m-1}^s$ at location $L_{n-1,m-1}$, and $\mathbf{L}_{n-1,m-1}$ is similar that $\mathbf{L}_{n-1,m-1} = [L_{n-1,m-1,1}, L_{n-1,m-1,2}, \dots, L_{n-1,m-1,H}]^T$. The label output data is $\mathcal{S}_{n,m}^Y = [s_{n,m,1}^Y, s_{n,m,2}^Y, \dots, s_{n,m,H}^Y]^T$ at location $L_{n,m}$.

C. SA-MDF-CNN Model

The network structure of SA-MDF-CNN is shown in Figure 3, mainly including attention module and convolutional network module. The first layer is the input layer, the size of which is $1976*6*8$, including 6 types of physical quantities (remote sensing SST, latitude, longitude, and the first 3 order eigenvectors) at 8 coordinates with a total depth of 1976 meters. The second layer is a flattening layer, which flattens the three-dimensional fusion data into one-dimensional sequence data as input for the self-attention layer. The third layer comes the self-attention layer, which converts the fusion data into query, key and value vectors through three linear transforms. Then, the dot product of each query vector and each key vector is calculated to obtain the attention score matrix, which is further converted into attention weights through softmax function. Finally, the value vectors are summed using attention weights to obtain the final output features. These layers are designed to enhance the model's ability of paying attention to the relationship between SSPs in different ocean areas in the input fusion data, so as to better capture the global dependence and key information between fusion data and the sound velocity distribution in the target ocean area.

The fourth and fifth layers are functional layers designed to reshape one-dimensional sequence data into two-dimensional data for subsequent feature extraction through convolution. The convolution layer is designed to further extract the features from the output data of the attention layer, which is better at capturing small-scale relationships of input features. The pooling layer is used to reduce the spatial dimension of the data, thereby reducing the number of parameters and reduce computational complexity, while retaining important feature information. The final two layers are the fully connected layer and the regression layer. The fully connected layer integrates the local features into the global features and outputs them to the regression layer. The RMSE is designed to be the loss function for calculating the gradient of the model parameters and updating weight parameters of the model through back propagation (BP) algorithm:

$$Loss = \sqrt{\frac{\sum_{h=1}^H (\hat{s}_{n,m,h}^Y - s_{n,m,h}^Y)^2}{H}}, \quad (9)$$

where $\hat{s}_{n,m,h}^Y$ is the estimated sound velocity value at depth h of location $L_{n,m}$, and the estimated SSP can be expressed as $\hat{S}_{n,m}^Y = [\hat{s}_{n,m,1}^Y, \hat{s}_{n,m,2}^Y, \dots, \hat{s}_{n,m,H}^Y]^T$. The SSP estimation algorithm based on SA-MDF-CNN is provided in Algorithm 1.

D. Multi-head self-attention module

The self-attention mechanism is a special type of attention mechanism used to process sequential data such as text, images, or time series. It allows the model to process the sequence in a way that considers the relationship between each element in the sequence and all other elements. The self-attention mechanism calculates weights by evaluating the similarities between different elements in a sequence to determine how much an element is related to other elements. Specifically, a kind of similarity score is defined to describe

Algorithm 1 The SSP estimation algorithm based on SA-MDF-CNN.

Require: Historical average SSP data $\mathcal{S}_{\mathcal{L}_x}^{mon}$, grid remote sensing SST $\mathcal{T}_{\mathcal{L}_x}^s$, position \mathcal{L}_x ;

- 1: Initialize the parameters θ , learning rate γ , and set the network parameters according to Table I;
- 2: **for** $k = 1$ to $MaxEpoch$ **do**
- 3: **for** $t = 1$ to $maxBatchSize$ **do**
- 4: Select a fusion data sample
- 5: $\mathcal{F}_{n-1,m-1}^X = [\mathbf{T}_{n-1,m-1}^S, \mathbf{L}_{n-1,m-1}, \mathcal{E}_{\mathcal{H},\mathcal{K}}]$;
- 6: $\mathcal{S}_{n,m}^Y = [s_{n,m,1}^Y, s_{n,m,2}^Y, \dots, s_{n,m,H}^Y]^T$;
- 7: $Loss_t = \sqrt{\frac{\sum_{h=1}^H (s_{n,m,h}^Y - \hat{s}_{n,m,h}^Y)^2}{H}}$;
- 8: $\hat{\theta} \leftarrow \text{Adam}(\nabla_{\theta} \frac{1}{BatchSize} \sum Loss_t, \theta, \gamma)$;
- 9: **end for**
- 10: **end for**
- 11: Complete training and save SA-MDF-CNN model;
- 12: Estimate and output target SSP $\mathcal{S}_{n,m}^{es}$ at intermediate coordinates $L_{n,m}^{test}$.

the similarity between each element in the sequence and other elements. Then, based on these similarity scores, the weight of each element can be calculated, and a weighted representation can be further obtained by multiplying the weight with the corresponding element. In order to better capture the associations between different types of SSP, multiple attention heads are used in this paper as shown in figure 4.

The diagram presented in Figure 4 illustrates the intricate workings of the multi-head self-attention mechanism, which is a fundamental building block in the architecture of transformer models. Three pivotal components are involved in the self-attention mechanism: the query \mathcal{Q} , key \mathcal{K} , and value \mathcal{V} vectors. These vectors are derived from the input data through linear transformations, as depicted in the upper right section of the diagram where the input is projected into the query, key, and value spaces using learnable weight matrices.

The query vector serves to assess the relevance or correlation with the key vectors. This correlation is quantified and utilized to compute a weighted sum, which amalgamates the contributions of the value vectors. The key vectors are instrumental in determining the attention distribution function, denoted as a_i in the diagram, which signifies the importance or weight of each element within the input sequence. In contrast, the value vectors encapsulate the specific features or numeric values associated with each element, playing a crucial role in the aggregation of information.

The mechanism operates by first computing the dot product between the query and each key vector. To prevent the dot products from growing too large and causing numerical instability, especially when the dimensionality of the keys d_k is high, each key is normalized by dividing it by $\sqrt{d_k}$. This normalization step is shown in the diagram as part of the attention calculation process. Following this, the softmax function is applied to the normalized dot products to generate a set of attention weights. These weights are then used to compute a weighted sum of the value vectors, as represented by the equation:

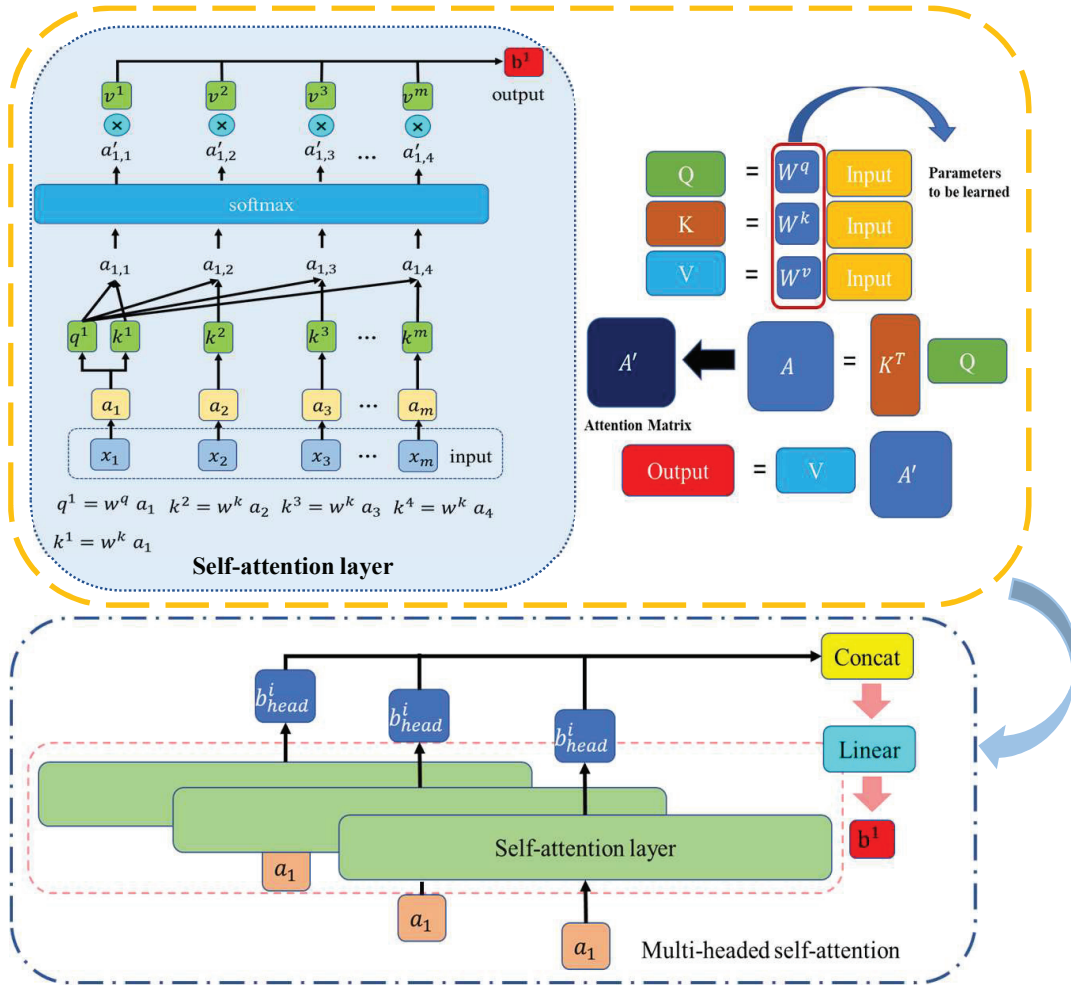


Fig. 4. The principle of the multi-head self-attention mechanism.

$$\text{Attention}(\mathcal{Q}, \mathcal{K}, \mathcal{V}) = \text{softmax} \left(\frac{\mathcal{Q}\mathcal{K}^T}{\sqrt{d_k}} \right) \mathcal{V} \quad (10)$$

This operation is performed for each head in the multi-head self-attention mechanism, as shown in the lower section of the diagram. Each head attends to different parts of the input sequence, allowing the model to capture a diverse range of dependencies and nuances within the data. The outputs from all heads are then concatenated and subjected to a linear transformation, resulting in the final output of the multi-head self-attention mechanism.

Given an input vector $\mathbf{x} \in \mathbb{R}^{dim}$, represented as $\mathcal{X} = [\mathbf{x}_1, \mathbf{x}_2, \dots, \mathbf{x}_M]$, where dim denotes the number of feature dimensions and M represents the number of sequence samples. Upon receiving a query vector \mathbf{q} , the self-attention function is defined as:

$$\text{att}(\mathcal{X}, \mathbf{q}) = \sum_{i=1}^M a_i \mathbf{x}_i = \sum_{i=1}^M \frac{\exp(s(\mathbf{k}_i, \mathbf{q}))}{\sum_{j=1}^M \exp(s(\mathbf{k}_j, \mathbf{q}))} \mathbf{v}_i, \quad (11)$$

where a_i is the i th attention weight, computed by the softmax function over the scaled dot product of the key vector \mathbf{k}_i

and the query vector \mathbf{q} . The function $s(\mathbf{k}_i, \mathbf{q})$ represents the similarity score between the key vector \mathbf{k}_i and the query vector \mathbf{q} , which is typically calculated as the dot product $\mathbf{k}_i^T \mathbf{q}$ divided by the square root of the key vector's dimension $\sqrt{d_k}$. The value vector \mathbf{v}_i corresponds to the i th sample in the input sequence, and the output of the self-attention function is a weighted sum of these value vectors, where the weights are determined by the attention mechanism.

In a standard self-attention module, the multi-head attention mechanism employs multiple query vectors \mathcal{Q} to select multiple sets of information from the input data in parallel. Specifically, each head independently computes the attention weights between the query vectors \mathcal{Q} , key vectors \mathcal{K} , and value vectors \mathcal{V} to extract different subsets of information. The output of the multi-head self-attention module is calculated by concatenating the outputs of all heads and then applying a linear transformation. The mathematical expression is:

$$\text{MultiHead}(\mathcal{Q}, \mathcal{K}, \mathcal{V}) = \text{Concat}(\text{head}_1, \dots, \text{head}_h) \mathcal{W}^O, \quad (12)$$

where $\text{head}_i = \text{Attention}(\mathcal{Q}\mathcal{W}_i^Q, \mathcal{K}\mathcal{W}_i^K, \mathcal{V}\mathcal{W}_i^V)$, $\mathcal{W}_i^Q \in \mathbb{R}^{d_k}$, $\mathcal{W}_i^K \in \mathbb{R}^{d_k}$, $\mathcal{W}_i^V \in \mathbb{R}^{d_v}$, and $\mathcal{W}^O \in \mathbb{R}^{hd_v}$ is a projection

of the parameter matrix.

IV. RESULTS AND DISCUSSIONS

To test the effectiveness of the proposed SA-MDF-CNN model, the monthly average fusion data from July 2015 to 2019 were selected as input training data and the monthly average SSP from 2020 were set to be the output label data. Experimental results were compared with other widely used methods for constructing spatial sound velocity distribution, including convolutional neural network (CNN), spatial interpolation (SITP) and mean values (MEAN), respectively. The model parameter settings are given in Table I.

TABLE I
PARAMETER SETTINGS OF SA-MDF-CNN

Parameter	Value
GPU	RTX 3090
input size	[1976,6,8]
self-attention	[8,32]
filter size	[2,2]
number of Channels	256
number of filters	256
convolution stride size	[1,1]
pool size	[2,2]
pooling stride	2
full connected output size	1976
minimum batch size	16
maximum epochs	100
learning rate	10^{-3}
drop factor of learning rate	0.1
drop period of learning rate	20

A. Accuracy Performance

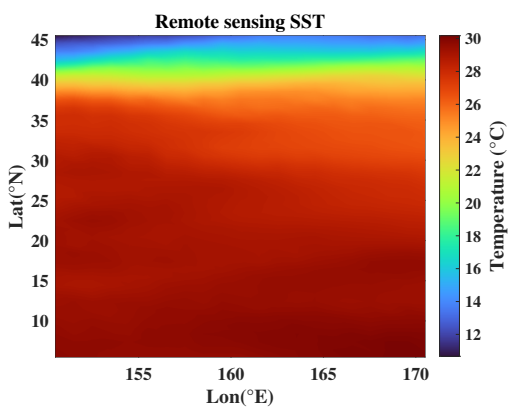


Fig. 5. Remote sensing SST data.

To test the accuracy performance of proposed model in estimating SSPs, real-time remote sensing SST data from different locations and depths were fused with EOF feature vectors to construct the sound velocity field. The remote sensing SST data are shown in figure 5, and a visual display of the fusion data is given in figure 6.

The real-time SSP estimation results of SA-MDF-CNN algorithm with depths ranging from 0 to 1976 meters within $7^{\circ}N$ to $28^{\circ}N$, $150^{\circ}E$ to $165^{\circ}E$ are compared with those of

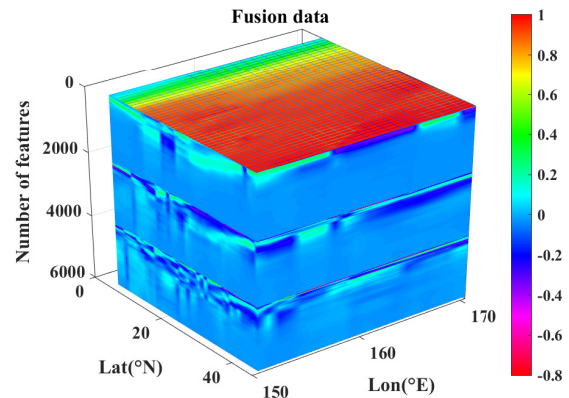


Fig. 6. Fusion data of remote sensing SST data, latitude and longitude coordinates, and EOF feature vectors.

CNN, SITP and mean values method as shown in figure 7. From the intuitive representation of the sound velocity heat-map, it can be seen that the sound velocity distribution estimated by SA-MDF-CNN and CNN has a significant improvement in accuracy compared to SITP and Mean value methods, and the estimated values of the proposed model are more similar to the sound velocity distribution of real samples. A comprehensive evaluation of the accuracy performance of various algorithms across different locations at depths ranging from 0 to 1976 meters is presented in Table II. Intuitive observation shows that the average RMSE results of SA-MDF-CNN, CNN, SITP, and Mean value methods are 0.1468, 0.1661, 0.2326, and 0.2447, respectively. Notably, the RMSE of SA-MDF-CNN for real-time SSP estimation is approximately 12% lower than that of CNN and approximately 30-40% lower than that of traditional SITP and mean value methods. Figure 8 gives a comparison of sound velocity estimation curves at $7.5^{\circ}N$, $156.5^{\circ}E$. In figure 8 (a), the curve of SA-MDF-CNN is the closest to the real SSP, and in figure 8 (b), the error mainly manifests in the shallow ocean area within 500 meters because the sound velocity in shallow water is more severely and irregularly affected by temperature. However, among all methods the error disturbance of SA-MDF-CNN is the smallest.

To further test the accuracy and performance of the model in estimating the sound velocity distribution in shallow water areas, the real-time SSP estimation results of SA-MDF-CNN algorithm at 200 m, 300 m and 500 m depths are compared with those of CNN, SITP and mean values method as shown in figure 9. As can be seen from the enlarged part of each sub-figure, the estimated SSP curves by SA-MDF-CNN at 200 m, 300 m and 500 m depths are significantly closer to the real SSP prediction results than those of CNN, SITP and mean method at the same ocean area. Specifically, an in-depth investigation into the performance of different algorithms in shallow ocean areas at varying depths and locations was conducted, with the real-time SSP estimation RMSE results compared and displayed in Table III. The largest RMSE is observed at a depth of 200 meters, which can be attributed to

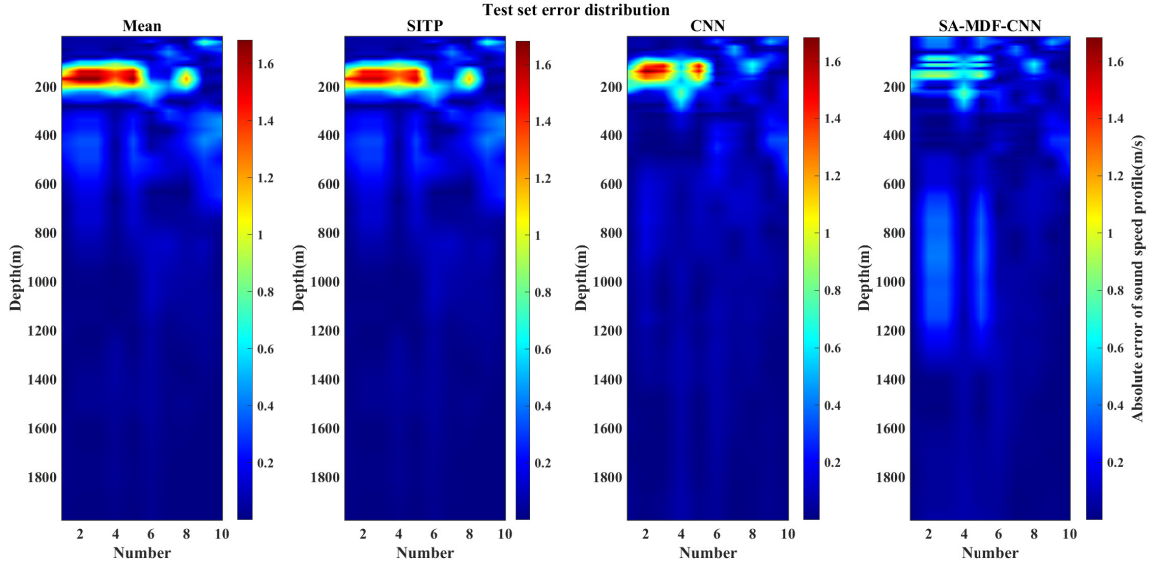


Fig. 7. Comparison of real-time estimated SSP results of different algorithms with depth of 1976 m, where (a) is the SA-MDF-CNN algorithm, (b) is the CNN algorithm, (c) is the spatial interpolation algorithm, and (d) is the mean value method.

TABLE II
COMPARISON OF RMSE AT THE SAME DEPTH:1976 METERS.

Number	Location	RMSE of different algorithms (m/s)			
		SA-MDF-CNN	CNN	SITP	Mean method
1	7.5°N 156.5°E	0.1125	0.1317	0.2456	0.2591
2	7.5°N 151.5°E	0.2599	0.3084	0.3182	0.3377
3	6.5°N 157.5°E	0.1293	0.1402	0.1730	0.1812
4	8.5°N 163.5°E	0.1152	0.1219	0.2775	0.2903
5	11.5°N 165.5°E	0.2090	0.2149	0.2709	0.2842
6	24.5°N 162.5°E	0.0787	0.1115	0.1232	0.1281
7	26.5°N 163.5°E	0.1181	0.1378	0.1293	0.1367
8	27.5°N 153.5°E	0.1039	0.1239	0.1532	0.1621
9	7.5°N 160.5°E	0.1945	0.2050	0.4025	0.4229
Average		0.1468	0.1661	0.2326	0.2447

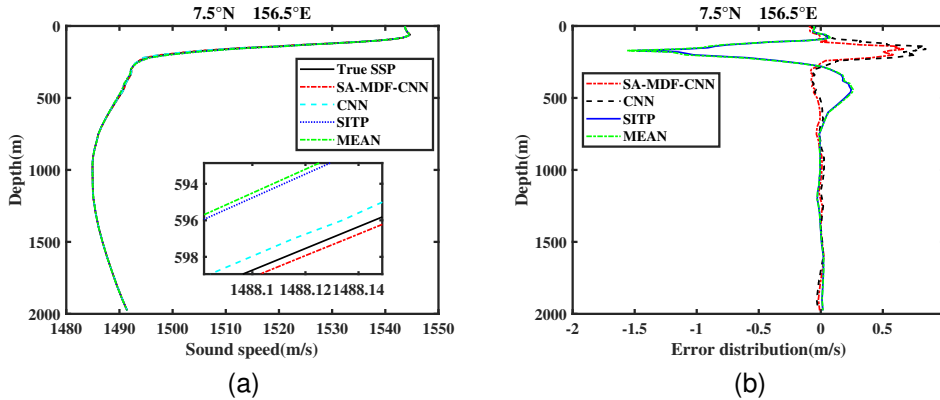


Fig. 8. A comparison example of real-time estimated SSP results of different algorithms with depths ranging from 0 to 1976 meters, where (a) is the comparison of estimated results and real SSP, and (b) is the comparison of error distribution between the estimated results of different algorithms and the real SSP.

the increased interference from real-time sea conditions in the shallow sea environment, such as wind speed, wave height, tsunami, and other factors. Concurrently, the experimental

results indicate that the estimation accuracy of the proposed SA-MDF-CNN model at 200 meters depth is enhanced by approximately 13% compared to CNN and by approximately

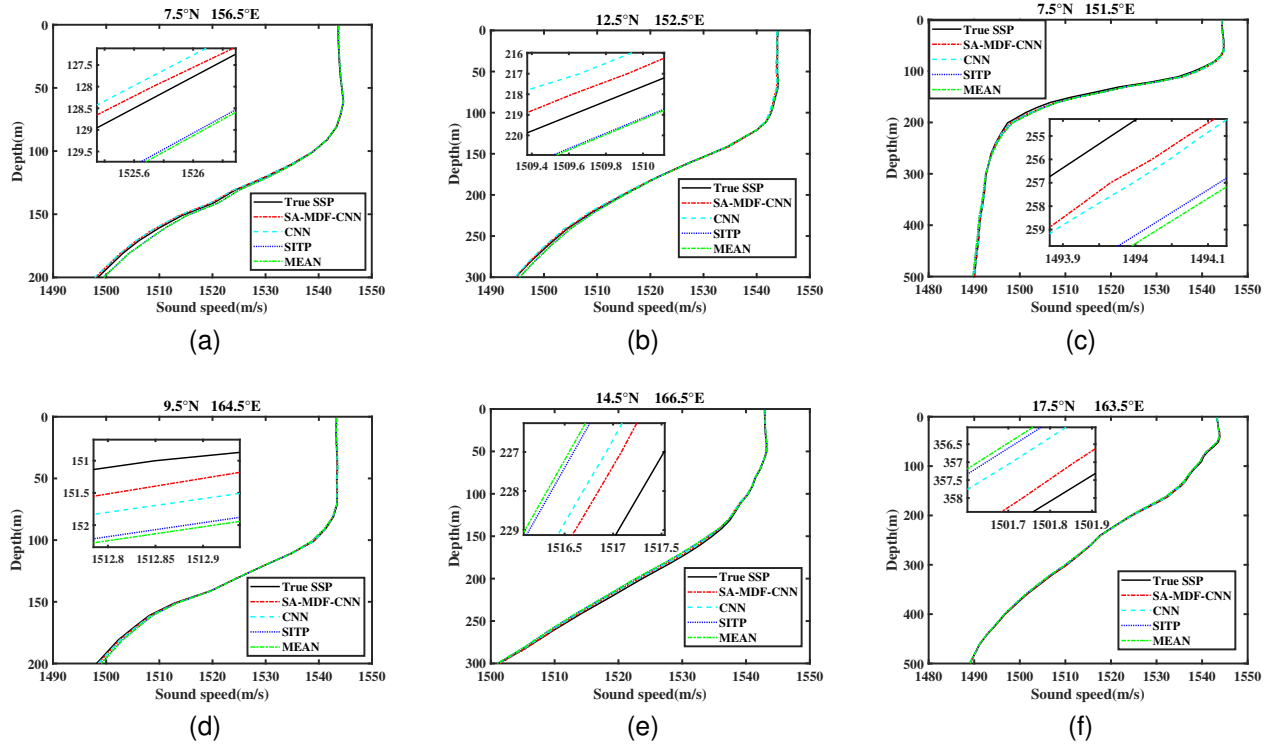


Fig. 9. Comparison of estimation results of different algorithms at different shallow ocean depths.

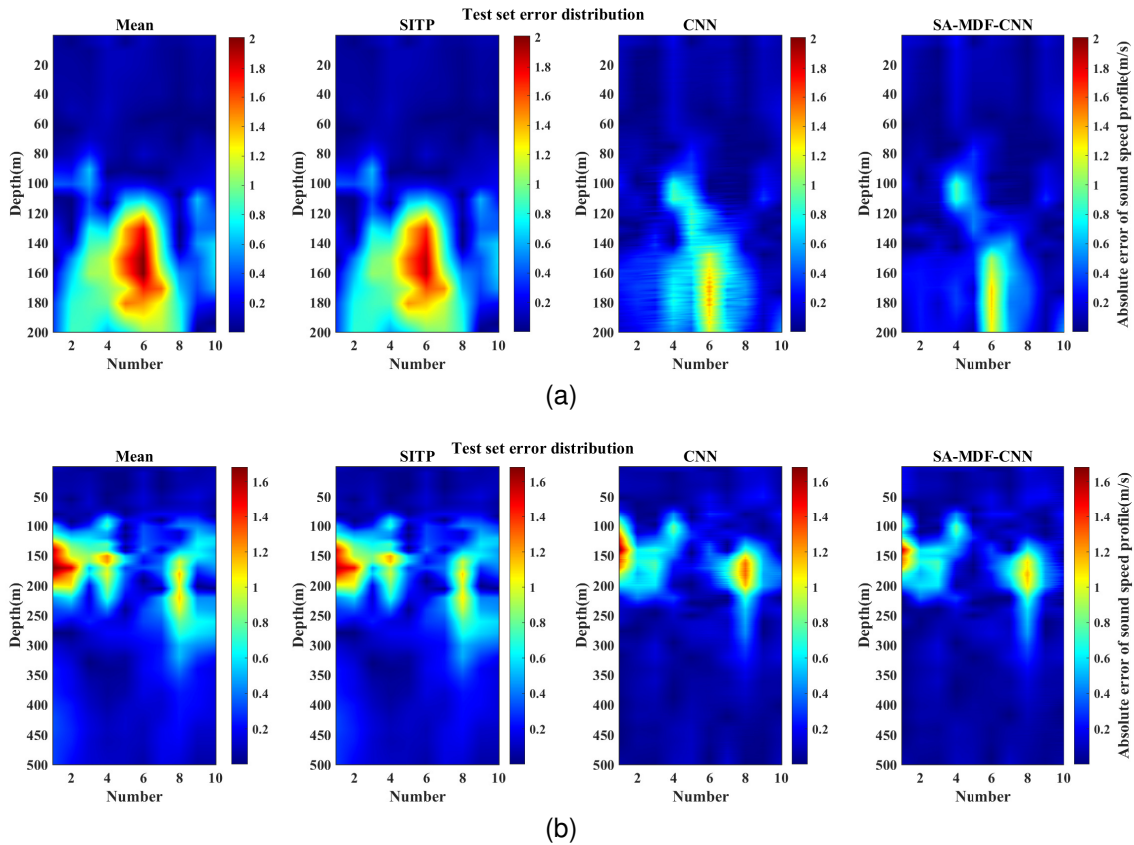


Fig. 10. Comparison of error distributions of real-time estimated SSPs for different algorithms at different shallow sea depths.

TABLE III
COMPARISON OF RMSE AT DIFFERENT DEPTH.

Depth	Location	RMSE of different algorithms (m/s)			
		SA-MDF-CNN	CNN	SITP	Mean method
200m	6.5°N 159.5°E	0.6075	0.6911	1.085	1.143
	7.5°N 156.5°E	0.2911	0.3468	0.6688	0.7035
	7.5°N 161.5°E	0.3859	0.4092	1.019	1.085
	9.5°N 164.5°E	0.1383	0.1775	0.3831	0.4018
	13.5°N 169.5°E	0.3115	0.3556	0.5565	0.5862
	Average	0.3469	0.3960	0.7425	0.7839
300m	11.5°N 165.5°E	0.4957	0.5155	0.6903	0.7240
	12.5°N 152.5°E	0.1901	0.3242	0.3392	0.3542
	13.5°N 154.5°E	0.2889	0.3028	0.4363	0.4594
	14.5°N 158.5°E	0.1360	0.1411	0.3860	0.4088
	14.5°N 166.5°E	0.2943	0.3446	0.5869	0.6156
	Average	0.2810	0.3256	0.4877	0.5124
500m	7.5°N 151.5°E	0.2293	0.2539	0.4839	0.5101
	6.5°N 157.5°E	0.2299	0.2613	0.3371	0.353
	8.5°N 164.5°E	0.2943	0.3257	0.6033	0.6368
	11.5°N 156.5°E	0.1571	0.1625	0.3331	0.3481
	17.5°N 163.5°E	0.1133	0.1841	0.2544	0.2721
	Average	0.2048	0.2375	0.4024	0.4240

53% compared to SITP and mean value method. At an ocean depth of 300 meters, the proposed algorithm demonstrates an improvement of about 14% over CNN and about 42% over SITP and mean value method. At 500 meters depth, the proposed model shows an improvement of about 14% compared to CNN and about 49% compared to SITP and mean value method. These experimental results collectively illustrate that the proposed model maintains significant precision advantages even in shallow sea environments of varying depths, thereby underscoring its applicability and effectiveness. The results indicate that SA-MDF-CNN is also applicable even in shallow ocean environment with different depths, and still has smaller RMSE compared with other algorithms, which means that the model still has good feature capture ability in shallow ocean scenes with significant changes in sound velocity. The average absolute error distribution comparison of real-time estimated SSP of different algorithms tested in the set of 200m and 500m depths is given in Figure 10. The error fluctuation of SA-MDF-CNN is the most stable, which indicates that SA-MDF-CNN still has better robust performance under shallow sea conditions with different depths.

B. Interpretability analysis

To investigate why the proposed SA-MDF-CNN model has better performance compared to CNN, we conducted an experiment and visually represented the attention weights of the model as shown in figure 11. Figure 11 (a) illustrates the first three order EOF feature vectors of the historical SSPs at various latitude and longitude coordinates. Figure 11 (b), (c), and (d) correspond to the attention weights when the training epochs are 10, 50, and 100, respectively. Through observing the evolution trend of attention focus with increasing training times, we found that the SA-MDF-CNN model increasingly focuses on the sound velocity distribution in shallow waters

within 1000 meters. This trend aligns with the first three orders of EOF feature distribution shown in panel (a), although the EOF itself emphasizes the SSP distribution between 0-500 meters. The attention depth of the proposed model spans 0-1500 meters, which is attributed to the variation of SSP distribution under different latitude and longitude coordinates. Therefore, in order to enhance the model's ability to focus on the global SSP distribution, we added a multi-head self-attention layer after input data fusion. This mechanism further confirms the effectiveness of the proposed model. Experiments based on the aforementioned public dataset demonstrate that the proposed SA-MDF-CNN model outperforms other algorithms in estimating sound velocity in both shallow and deep waters.

C. Efficiency and stability

TABLE IV
COMPARISON OF NEURAL NETWORKS

Network	Number of Parameter	Train time
CNN	61.9M	72s
SA-MDF-CNN	149M	40s

Although the accuracy performance in SSP estimation of SA-MDF-CNN is better than traditional methods, the disadvantage is that SA-MDF-CNN increases the number of parameters and computational overhead. Table IV shows the comparison of parameters and running time between the proposed model and CNN. It can be seen that the proposed model in this paper needs more parameters and training time than CNN, which is a necessary overhead for performance improvement.

To test the stability of the model, the convergence of SA-MDF-CNN and CNN with different numbers of iteration

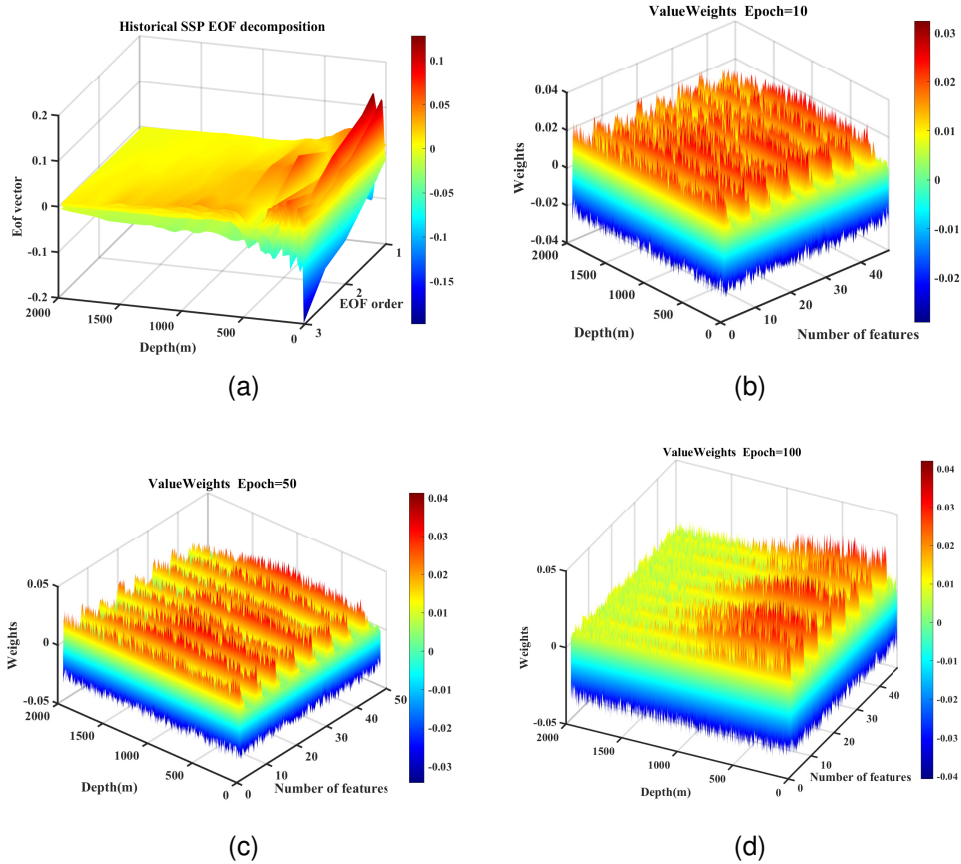


Fig. 11. Interpretability analysis of the SA-MDF-CNN model, where (a) is the first three order EOF the historical SSP at different positions (b) is the attention weight with Epoch=10, (c) is the attention weight with Epoch=50, and (d) is the attention weight at Epoch=100.

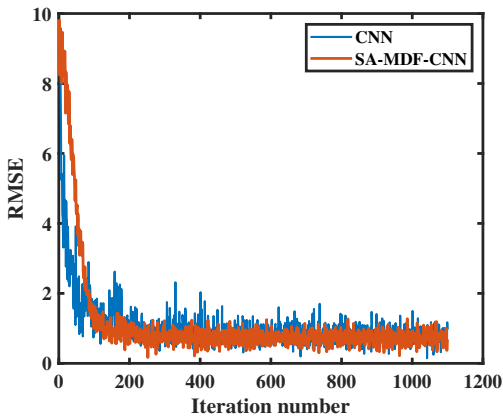


Fig. 12. Comparison of RMSE convergence of different algorithms.

is given in figure 12. Both SA-MDF-CNN and CNN can converge in less than 200 training iterations. The convergence of SA-MDF-CNN is smoother than that of CNN, which may be due to the multi-head self-attention mechanism focusing more on global features and therefore not causing significant parameter updates due to drastic changes in a small range of the data.

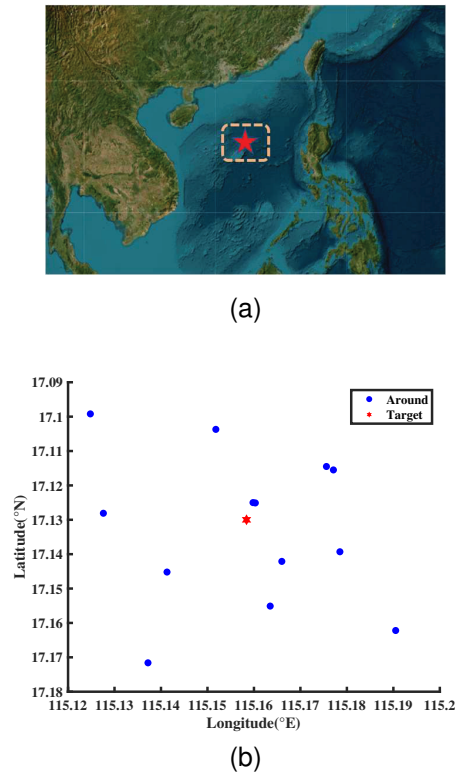
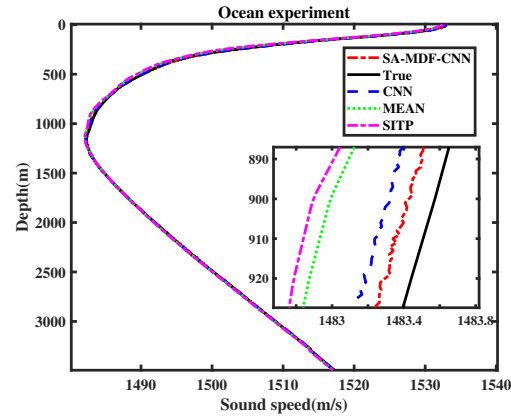
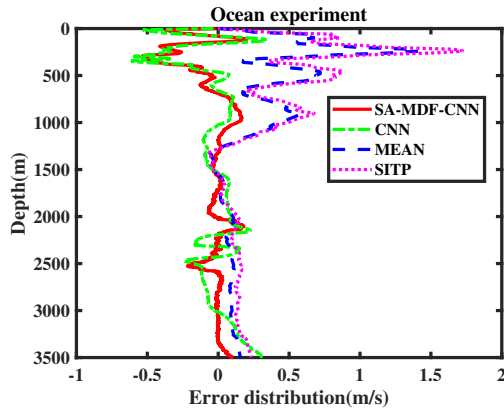


Fig. 13. Data sampling locations of ocean experiments.



(a)



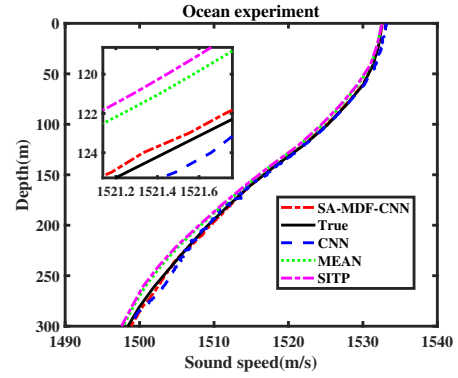
(b)

Fig. 14. Comparison of real-time SSP estimation results of different algorithms on ocean experimental data, where (a) shows the SSP curves, and (b) shows the error distributions.

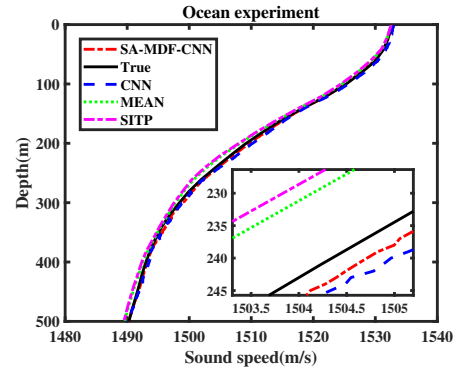
V. OCEAN EXPERIMENTS

In order to verify the practicality of the SA-MDF-CNN model, a comprehensive deep-ocean experiment was conducted in the South China Sea in April 2023. As illustrated in figure 13 (a), various instruments such as CTD and XCTD were employed at diverse marine locations, yielding a total of 14 distinct samples. The depth of sampling reached 3500 meters, with intervals set at every 100 meters. It is evident that the selected location for this experiment does not conform to the rigid 3x3 grid pattern, thus allowing for a more rigorous evaluation of the proposed model. The fusion data at the blue coordinates in figure 13 (b) were selected as the input of the model, and the real-time SSP under the red pentagram was used as the prediction output of the model.

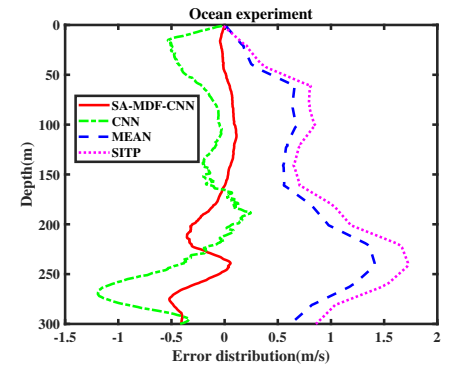
To evaluate the effectiveness of the model in estimating the distribution of sound velocity at full-ocean depth, the estimated SSP of SA-MDF-CNN is compared with other algorithms in figure 14. It is evident that the proposed model exhibits lower RMSE and more stable error disturbance compared to traditional algorithms and CNN. To further test the sound velocity estimation performance in shallow waters with significant changes in sound velocity, estimation of sound velocity at 300, 500 depth meters by SA-MDF-CNN are compared



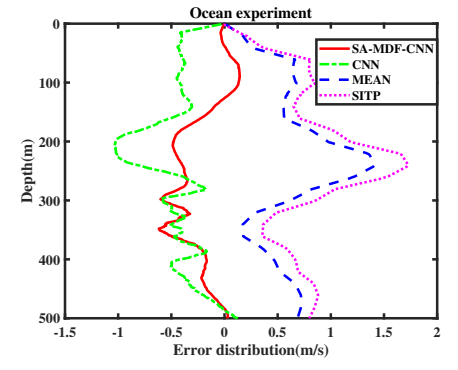
(a)



(b)



(c)



(d)

Fig. 15. Comparison of real-time estimation SSP results of different algorithms in shallow sea environment with different depths in ocean experiment, where (a) and (c) are SSP curves of 300 meters depth, (b) and (d) are error distributions of 500 meters depth.

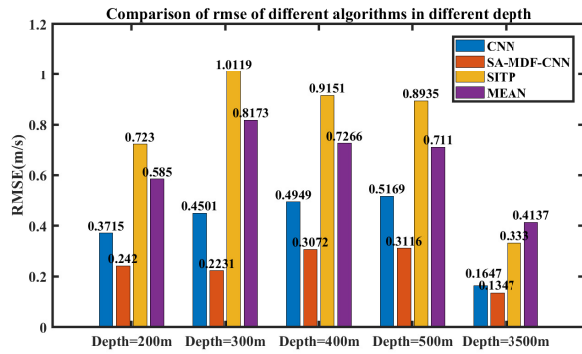


Fig. 16. RMSE comparison of real-time estimated SSPs by different algorithms of ocean experiments.

with other methods in figure 15. The results indicate that the proposed algorithm has smaller error disturbances and maintains significant accuracy advantages compared to other algorithms in shallow water environments. Figure 16 gives a more detailed comparison of the RMSE results of different algorithms, clearly showing that the proposed model has significant advantages at different depths.

VI. CONCLUSION

To construct a real-time sound velocity field and eliminate the need for underwater onsite data measurement operations, a SA-MDF-CNN model driven by multimodal data fusion is proposed in this paper, which fuses historical SSP features, real-time remote sensing SST, latitude and longitude coordinates. The fusion data is constructed by gridding, and the real-time SSP is retrieved based on the real-time remote sensing SST. The effectiveness of our proposed model was tested in the case of non-standardized grid through ocean experiments. The experimental results show that our proposed model is not only suitable for real-time SSP estimation under non-strictly standardized grid conditions, but also suitable for shallow sea conditions with different depths.

ACKNOWLEDGMENTS

The authors acknowledge the historical SSP data support from the China Argo Real-time Data Center, (<https://www.argo.org.cn/>, latest access: December 20, 2024). The remote sensing SST data can be acquired at the National Oceanic and Atmospheric Administration (<https://www.commerce.gov/>, latest access: December 25, 2024).

REFERENCES

- [1] M. Erol-Kantarci, H. T. Mouftah, and S. Oktug, "A survey of architectures and localization techniques for underwater acoustic sensor networks," *IEEE Commun. Surv. Tutor.*, vol. 13, no. 3, pp. 487–502, Mar., 2011.
- [2] J. Luo, Y. Yang, Z. Wang, and Y. Chen, "Localization algorithm for underwater sensor network: A review," *IEEE Internet Things J.*, vol. 8, no. 17, pp. 13 126–13 144, Sep., 2021.
- [3] A. Jehangir, S. M. Majid Ashraf, R. Amin Khalil, and N. Saeed, "Isac-enabled underwater iot network localization: Overcoming asynchrony, mobility, and stratification issues," *IEEE Open J. Commun. Soc.*, vol. 5, pp. 3277–3288, May, 2024.
- [4] W. Huang, M. Liu, D. Li, F. Yin, H. Chen, J. Zhou, and H. Xu, "Collaborating ray tracing and ai model for auv-assisted 3-d underwater sound-speed inversion," *IEEE J. Ocean. Eng.*, vol. 46, no. 4, pp. 1372–1390, May, 2021.
- [5] T. Zhang, L. Yan, G. Han, and Y. Peng, "Fast and accurate underwater acoustic horizontal ranging algorithm for an arbitrary sound-speed profile in the deep sea," *IEEE Internet Things J.*, vol. 9, no. 1, pp. 755–769, Jun., 2022.
- [6] X. Yu, H.-D. Qin, and Z.-B. Zhu, "Underwater localization of auvs in motion using two-way travel time measurements with unknown sound velocity," *IEEE Trans. Veh. Technol.*, vol. 72, no. 9, pp. 11 358–11 373, May, 2023.
- [7] Y. Liu, Y. Wang, C. Chen, and C. Liu, "Unified underwater acoustic localization and sound speed estimation for an isogradient sound speed profile," *IEEE Sens. J.*, vol. 24, no. 3, pp. 3317–3327, Dec., 2024.
- [8] J. Bonnel, S. P. Pecknold, P. C. Hines, and N. R. Chapman, "An experimental benchmark for geoacoustic inversion methods," *IEEE J. Ocean. Eng.*, vol. 46, no. 1, pp. 261–282, Jan., 2021.
- [9] J. Bonnel, A. R. McNeese, P. S. Wilson, and S. E. Dosso, "Geoacoustic inversion using simple hand-deployable acoustic systems," *IEEE J. Ocean. Eng.*, vol. 48, no. 2, pp. 592–603, Nov., 2023.
- [10] P. Wu, J. Sun, G. Shan, Z. Sun, and P. Wei, "Inversion of deep-water velocity using the munk formula and the seabed reflection traveltime: An inversion scheme that takes the complex seabed topography into account," *IEEE Trans. Geosci. Remote Sensing*, vol. 61, pp. 1–14, May, 2023.
- [11] W. Huang, P. Wu, J. Lu, J. Lu, Z. Xiu, Z. Xu, S. Li, and T. Xu, "Underwater ssp measurement and estimation: A survey," *J. Mar. Sci. Eng.*, vol. 12, no. 12, Dec., 2024.
- [12] X. Feng, C. Chen, and K. Yang, "An estimation method for sound speed profile based on large depth array multipath delay," *IEEE Geosci. Remote Sens. Lett.*, vol. 21, pp. 1–5, Jun., 2024.
- [13] A. Tolstoy, O. Diachok, and L. N. Frazer, "Acoustic tomography via matched field processing," *J. Acoust. Soc. Am.*, vol. 89, no. 3, pp. 1119–1127, 03 Mar., 1991.
- [14] Y. Choo and W. Seong, "Compressive sound speed profile inversion using beamforming results," *Remote Sens.*, vol. 10, no. 5, May, 2018.
- [15] M. Bianco and P. Gerstoft, "Dictionary learning of sound speed profiles," *J. Acoust. Soc. Am.*, vol. 141, no. 3, pp. 1749–1758, 03 Mar., 2017.
- [16] W. Huang, D. Li, H. Zhang, T. Xu, and F. Yin, "A meta-deep-learning framework for spatio-temporal underwater ssp inversion," *Front. Mar. Sci.*, vol. 10, Aug., 2023.
- [17] Y. Liu, B. Ma, Z. Qin, C. Wang, C. Guo, S. Yang, J. Zhao, Y. Cai, and M. Li, "A multi-spatial scale ocean sound speed prediction method based on deep learning," *J. Mar. Sci. Eng.*, vol. 12, no. 11, Oct., 2024.
- [18] J. Lu, W. Huang, and H. Zhang, "Dynamic prediction of full-ocean depth ssp by a hierarchical lstm: An experimental result," *IEEE Geosci. Remote Sens. Lett.*, vol. 21, pp. 1–5, Jan., 2024.
- [19] X. Cui, X. Liu, J. Li, L. Li, B. Jiang, S. Li, and J. Liu, "Adaptive sound velocity profile prediction method based on deep reinforcement learning," *IEEE Sens. Lett.*, vol. 8, no. 3, pp. 1–4, Feb., 2024.
- [20] B. Huang, C. Liu, V. Banzon, E. Freeman, G. Graham, B. Hankins, T. Smith, and H. Zhang, "Improvements of the daily optimum interpolation sea surface temperature (doisst) version 2.1," *J. Clim.*, vol. 34, no. 8, pp. 2923 – 2939, Apr., 2021.
- [21] G. Xu, K. Qu, Z. Li, Z. Zhang, P. Xu, D. Gao, and X. Dai, "Enhanced inversion of sound speed profile based on a physics-inspired self-organizing map," *Remote Sens.*, vol. 17, no. 1, Jan., 2025.
- [22] K. Kirimoto, J. Han, and S. Konashi, "Development of high accuracy ctd sensor: 5el-ctd," in *OCEANS 2024 - Singapore*, 2024, pp. 1–8.
- [23] C. Luo, Y. Wang, C. Wang, M. Yang, and S. Yang, "Analysis of glider motion effects on pumped ctd," in *OCEANS 2023 - Limerick*, 2023, pp. 1–7.
- [24] W. Munk and C. Wunsch, "Ocean acoustic tomography: a scheme for large scale monitoring," *Deep-Sea Res. Part I-Oceanogr. Res. Pap.*, vol. 26, no. 2, pp. 123–161, Feb., 1979.
- [25] —, "Ocean acoustic tomography: Rays and modes," *Rev. Geophys.*, vol. 21, no. 4, pp. 777–793, May, 1983.
- [26] W. Zhang, S.-e. Yang, Y.-w. Huang, and L. Li, "Inversion of sound speed profile in shallow water with irregular seabed," *AIP Conf. Proc.*, vol. 1495, no. 1, pp. 392–399, 11 Nov., 2012.
- [27] M. Zhang, W. Xu, and Y. Xu, "Inversion of the sound speed with radiated noise of an autonomous underwater vehicle in shallow water waveguides," *IEEE J. Ocean. Eng.*, vol. 41, no. 1, pp. 204–216, Apr., 2016.

- [28] M. Reichstein, G. Camps-Valls, B. Stevens, M. Jung, J. Denzler, N. Carvalhais, and Prabhat, "Deep learning and process understanding for data-driven earth system science," *Nature*, vol. 566, pp. 195–204, Feb., 2019.
- [29] M. Jahanbakht, W. Xiang, L. Hanzo, and M. Rahimi Azghadi, "Internet of underwater things and big marine data analytics—a comprehensive survey," *IEEE Commun. Surv. Tutor.*, vol. 23, no. 2, pp. 904–956, Jan., 2021.
- [30] X. Yu, T. Xu, and J. Wang, "Sound velocity profile prediction method based on rbf neural network," in *China Satellite Navigation Conference (CSNC) 2020 Proceedings: Volume III*. Singapore: Springer Singapore, Jun., 2020, pp. 475–487.
- [31] R. W. Reynolds, T. M. Smith, C. Liu, D. B. Chelton, K. S. Casey, and M. G. Schlax, "Daily high-resolution-blended analyses for sea surface temperature," *J. Clim.*, vol. 20, no. 22, pp. 5473 – 5496, Nov., 2007. [Online]. Available: <https://journals.ametsoc.org/view/journals/clim/20/22/2007jcli1824.1.xml>
- [32] C. Xie, X. Miaomiao, and S. Cao, "Gridded argo data set based on gdcsm analysis technique: establishment and preliminary applications," *Journal of Marine Sciences*, vol. 37, no. 4, pp. 24–35, 2019.